Colloids and Surfaces A: Physicochem. Eng. Aspects 490 (2016) 98–103

Contents lists available at ScienceDirect

Colloids and Surfaces A: Physicochemical and Engineering Aspects

journal homepage: www.elsevier.com/locate/colsurfa

Iron oxide nanoparticles prepared by laser ablation: Synthesis, structural properties and antimicrobial activity

Enza Fazio[a,*], Marco Santoro[a], Germana Lentini[b], Domenico Franco[b], Salvatore Pietro Paolo Guglielmino[b], Fortunato Neri[a]

[a] Dipartimento di Scienze Matematiche e Informatiche, Scienze Fisiche e Scienze della Terra, Università di Messina, Viale Ferdinando Stagno d'Alcontres 31, 98166 Messina, Italy

[b] Dipartimento di Scienze Chimiche, Biologiche, Farmaceutiche ed Ambientali, Università di Messina, Viale Ferdinando Stagno d'Alcontres 31, 98166 Messina, Italy

HIGHLIGHTS

- Iron oxide nanoparticles embedded in a polymeric matrix.
- Iron oxide nanoparticles synthesized by a high-power picosecond laser.
- Effects of PVA on Fe_2O_3 nanoparticles distribution and dimensionality.
- Fe_2O_3 nanoparticles toxicity on *Staphylococcus aureus*.
- Fe_2O_3 nanoparticles as vectors for drug targeting platforms.
- Antimicrobial activity by MTT assay.

GRAPHICAL ABSTRACT

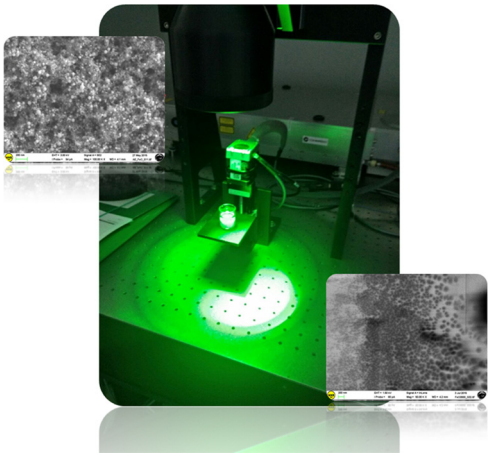

ARTICLE INFO

Article history:
Received 31 July 2015
Received in revised form 7 November 2015
Accepted 16 November 2015

Keywords:
Iron oxide nanoparticles
Staphylococcus aureus
PVA water solution
Picosecond laser source
STEM
MTT assay

ABSTRACT

Pulsed laser ablation of iron rod target in water-based solutions were carried out, varying the ablation parameters. The structural, morphological and compositional characteristics of the nanoparticles were studied by micro-Raman, dynamic light scattering (DLS), X-ray photoelectron (XPS) spectroscopies and electron scanning microscopy (SEM/STEM). Slight changes in the ablation parameters result in significant variations in the nanoparticles morphology. As observed by STEM imaging, particles size and distribution was tuned from agglomerated to nearly spherical structures, mainly changing the medium (water or polyvinyl alcohol PVA water solution). On the other hand, the polymeric phase increases the iron oxide nanoparticles stability, biocompatibility and interactive functions on the surface. Antimicrobial activity of iron oxide nanoparticles on *Staphylococcus aureus* was studied by means of MTT assay. The results indicate that the iron oxide nanoparticles are interesting for potential applications as vector for drug delivery and as constituent of specific platforms for drug targeting.

1. Introduction

In the rapidly emerging field of nanopiotechnology, metal nanoparticles (MNPs) are extensively used in drug delivery [1],

* Corresponding author. Fax: +39 090 676 5458.
E-mail address: enfazio@unime.it (E. Fazio).

http://dx.doi.org/10.1016/j.colsurfa.2015.11.034
0927-7757/

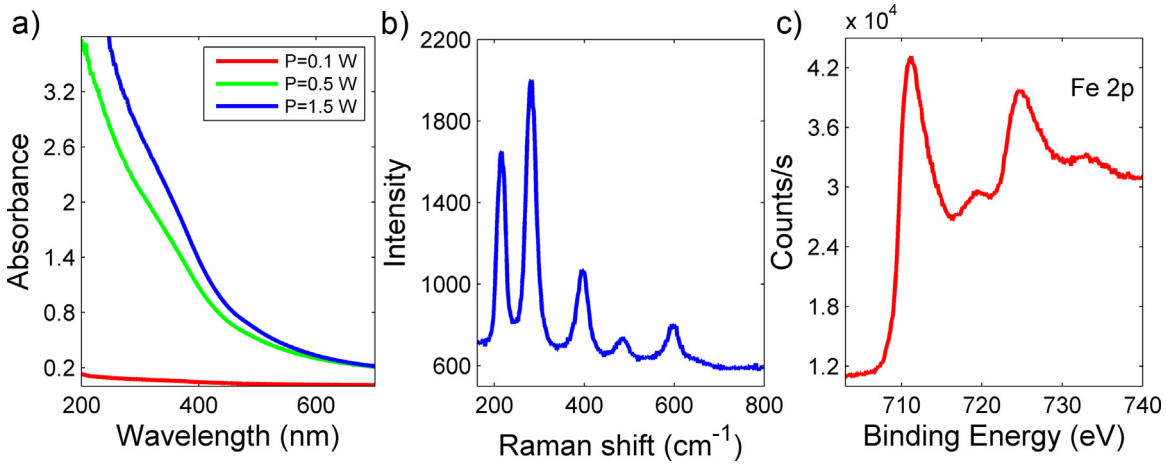

Fig. 1. (a) Optical absorption spectra of the iron oxide nanocolloids prepared in water, varying the laser power; (b) Raman spectrum and (c) Ag 3d XPS photoemission spectra of the sample prepared in water, at the laser power of 0.5 W, for an ablation time of 2 min.

biosensors [2], bio-imaging [3], antimicrobial activities [4] and food reservation [5], by exploiting their unique physical chemical and biological properties. Their nanoscale size, three-dimensional structure, large surface area and negligible side effects make them highly effective for biomedical applications such as molecular imaging [3] and cancer therapy [6]. Nontoxic superparamagnetic magnetic nanoparticles with functionalized surface coatings can conjugate chemotherapeutic drugs or active molecules which can be released on a specific target manipulating the MPs by an external magnetic field. The effect of size and surface coating of magnetic nanoparticles are very important for their role as diagnostic and therapeutic agents [7]. Iron oxide has been widely used in biomedical research because of its biocompatibility and magnetic properties. Iron oxide nanoparticles, with sizes less than 100 nm, have been developed as contrast agents for magnetic resonance imaging [8] as hyperthermia agents [9] and as carriers for targeted drug delivery to treat several types of cancer [10], by using an external magnetic field to direct FeO nanoparticles to desirable sites (such as implant infection) for immediate treatment. Several studies report that iron nanoparticles exhibit antibacterial activity in dependence of their size, concentration and oxidation state [11]. Antimicrobial activity of the nanoparticles is known to be a function of the surface area in contact with the microorganisms. The ions released by the nanoparticles may attach to the negatively charged bacterial cell wall and rupture it, thereby leading to protein denaturation and cell death [12]. Xiu et al. [13] found that the anaerobic dechlorinating bacteria *Dehalococcoides* sp. was sensitive to nanoscale zero valent iron exposure when they studied the bioremediation of trichloroethylene, using a mixture of bacterial species. Increasing the Fe nanoparticles concentration substantially inhibited the growth of *Escherichia coli* and *Staphilococcus aureus* [14]. Recent attention has been turned to the development of synthetic procedures that are environmentally friendly in order to minimize chemical waste as well as potential safety issues associated. On the other hand, the attention is focused to fully understand the interaction mechanisms between iron oxide nanoparticles and living systems.

The present study is focused on the synthesis of iron oxide nanocolloids by means of a picoseconds pulsed laser ablation technique. This latter is a fast and clean technique which allowed the formation of chemically and morphologically stable Fe_2O_3 nanocolloids with a narrow size distribution. Our technological challenge was been to optimize the ablation process parameters that make the Fe_2O_3 nanostructures stable, both at rest and under high light/magnetic flux, with a narrow size distribution and to assess their antibacterial activity.

2. Material and methods

Pulsed laser ablation of high purity (99.9%) iron rod target in pure water (H_2O) and in PVA water solution has been carried out using the second harmonic (532 nm) of a laser operating at 100 kHz repetition rate with a pulse width of 6–8 ps. The target was irradiated for typical laser power of 0.1 0.5 and 1.5 W and an irradiation time of 16 min in water. The ablation processes in the PVA water solution were carried out also with steps of 1 min for a total time of ablation of 16 min, by spending 10 min between an ablative process and the other one. The PVA water solution has so been obtained: 7.5 gr of PVA (PM = 86,000) are dissolved in 30 mL of distilled water. The dispersion was heated up to the temperature of 90 °C and, subsequently, left to reflux under magnetic agitation for 2 h; then, cooled down to room temperature. The dispersion was further diluted in water to obtain a 7.5% P/V final solution. The iron oxide content was estimated to be about 0.2% P/V.

The micro-Raman responses of the materials were investigated after the deposition of some drop of the water colloids on a CaF_2 substrates. Raman spectra were excited by the 638 nm radiation of a 30 mW diode laser, for an integration time of 80 s. The backscattered radiation, collected by an Olympus BX 40 microscope optics using a 50X objective lens, was analyzed by an XploRA 1800 cm^{-1} monochromator equipped with a Peltier CCD sensor. The optical transmission of the iron oxide colloids was analyzed by means of a PerkinElmer Lambda 750 UV–vis spectrometer in the 190–1100 nm range, using quartz cells. The size of the nanoparticles was determined by dynamic light scattering (DLS) measurements using a Horiba NanoParticle Analyzer SZ-100 (range: 0.3 nm–8 μm). Using the same Horiba NanoParticle Analyzer SZ-100, the Zeta potential was quantified with a laser Doppler method, based on the principle of electrophoretic mobility under an electric field. A fraction of the same colloids was deposited on carbon substrates to carry out Scanning Electron Microscopy (SEM) characterization. SEM images were taken by a scanning electron microscope (Merlin; model ZEISS-Gemini 2) operating at an accelerating voltage of 30 kV and at a working distance of 4 mm when the measure was carried out in transmission mode (STEM) and at an accelerating voltage of 3 kV for the collection of the SEM images. X-ray photoelectron spectroscopy (XPS) spectra were acquired using a K-Alpha system of Thermo Scientific, equipped with a monochromatic Al-Kα source (1486.6 eV) and operating in constant analyzer energy (CAE) mode

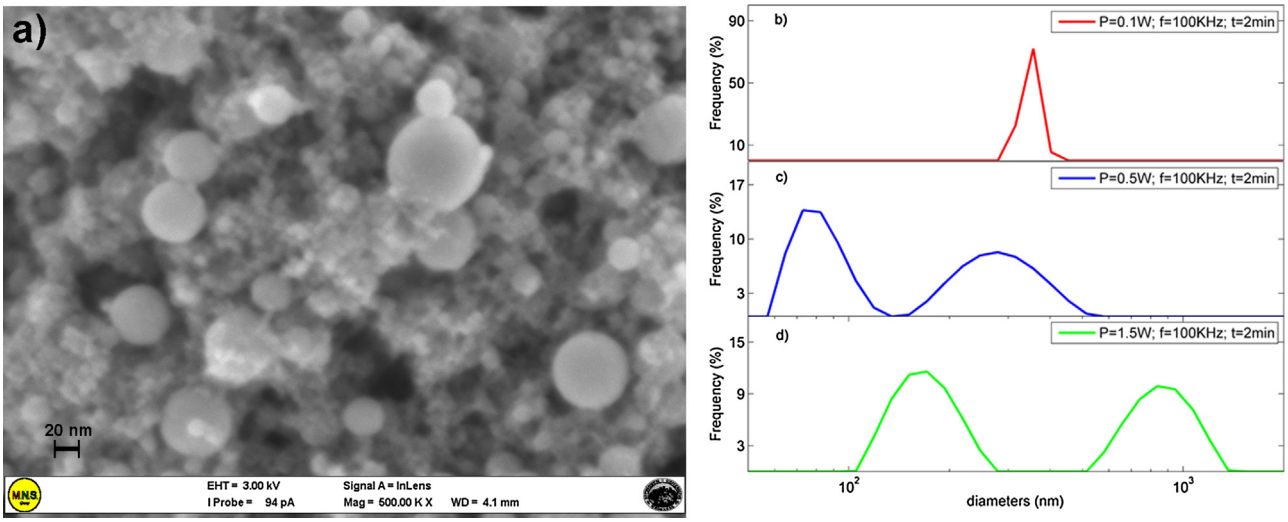

Fig. 2. SEM image of the sample prepared in water at the laser power of 0.5 W (a) and the iron oxide particles diameters distribution estimated by DLS data (b).

with a pass energy of 20 eV for high resolution spectra and a spot size of 400 mm.

Nanoparticles antimicrobial activity was tested against *S. aureus* ATCC 29213 (*S. aureus*), from the American Type Culture Collection (ATCC). Stock organisms were maintained in Trypticase Soy Broth (TSB) containing 20% (v/v) glycerol at −80 °C. MTT [3-(4,5-dimethylthiazol-2-yl)-2,5-diphenyltetrazolium bromide, Sigma M-5655] was purchased from Sigma–Aldrich (St. Louis, MO). MTT was dissolved in distilled water to a concentration of 5.0 g/L and stored in 1.5-mL centrifuge tubes at −20 °C. A single colony of *S. aureus* was inoculated into 10 mL of Muller Hinton Broth (MHB, 70192 Fluka). Bacteria were incubated at 37 °C in an orbital shaker–incubator (350 rpm, ARGOLab SXO-D-XL) for another about 14 h. Then, the bacteria solution was diluted in MHB and incubated at 37 °C under agitation at 350 rpm. The pH was not adjusted during the course of cultivation. *S. aureus* cell growth was monitored by measuring the optical density of the broth at 600 nm (OD_{600}). After three hours, bacterial culture shows an optical density (OD) of 0.9 at 600 nm. According to the standard curve correlating bacteria number with optical density, this value was equivalent to 5×10^6 cells/mL. Iron oxide nanoparticles, both in water or PVA aqueous solutions, were added to bacteria cultures. A culture of bacteria without nanoparticles served as control. MTT reduction assay was carried out according to the procedure described by Wang et al. [15]. To initiate the reduction reaction, 20 μL of 5 g/L MTT stock solution was added to 200 μL of each sample (diluited to OD_{600} 0.01–0.18 in MHB) and the mixtures were incubated at 37 °C with the tube cap open for 20 min. The formazan crystals produced were collected by centrifugation of the 1.5-mL centrifuge tubes at 10,000 × *g* for 1 min (Eppendorf Centrifuge 5418) and the medium was pipetted off without shaking. The supernatant was discarded and the pellets resuspended in 2500 μL of DMSO (DMSO, RudiPont 11836-11) and the tubes were vortexed. The formazan crystals were dissolved at room temperature. The ODs were measured using DMSO as the blank. In this case, the absorbance values at 550 nm (A_{550}) was collected for monitoring formazan production. The MTT reduction activities of *S. aureus* cells were presented as MTT reduction unit (MRU) per OD_{600} and per milliliter culture. One MTT reduction unit (MRU) is defined as an A_{550} value of 1.0 produced by the dissolved formazan crystals from the cells in the medium at 37 °C in 20 min. All experiments were conducted in triplicate and repeated three times.

3. Results and discussion

3.1. Structural and morphological analyses

Being known that the nature of antibacterical response depends on the structural and morphological properties of the iron oxide nanoparticles, it is of paramount importance to determine the appropriate ablation parameters to obtain nanoparticles with tailored size distributions and concentration. Hence, first we investigated the effects of the solvent level above the target and the optical system positions on the ablated spot which, in turn, determines the operative fluence. Now, to discerne the appropriate conditions (in terms of the optical system position and water level) to obtain the higher nanoparticles productivity, we carried out the ablation processes at the fixed laser power of 0.1 W and for an ablation time of 2 min, varying the water thickness and the distance between the target and the optical system. The iron oxide nanoparticles concentration were indirectly estimated carrying out optical absorption measurements in the UV–vis spectral region (not shown) and also collecting, by means of a magnet, the particles on the wall of the vial containing the colloidal solution. Then, the iron oxide solid phase is weighed. It emerges that the higher iron oxide particles concentration was obtained when the level above the target is 5 mm and the target-optical system distance is 40 mm. Then, we carried out an ablation process for a time of 5 min. The obtained colloidal solution falls only after a few minutes. Hence, the optimal ablation time is of 2 min. Therefore, keeping fixed the ablation parameters for which we found the highest productivity of particles, we carried out the ablation processes varying the laser power between 0.1 and 1.5 W (Fig. 1).

The optical characteristic of the colloids vs the laser power are shown in Fig. 2. The optical absorption spectra in the 190–1000 nm are not generally representative of the iron oxide nanoparticles occurred formation, since there is not a well defined absorbance band in this spectral region. However, the optical absorbance spectrum is characterized by an absorption threshold for wavelength lower than 400 nm, typical of different iron oxide phase (hematite α-Fe_2O_3, maghemite γ-Fe_2O_3 or Fe_3O_4) as well as of the Fe_3—C bonds [16].

On the overall, the optical absorption spectra give indirectly semi-quantitative informations of the nanoparticles concentrations, fixed the ablation time, varying the laser power. The higher nanoparticles concentration is obtained at the higher laser power

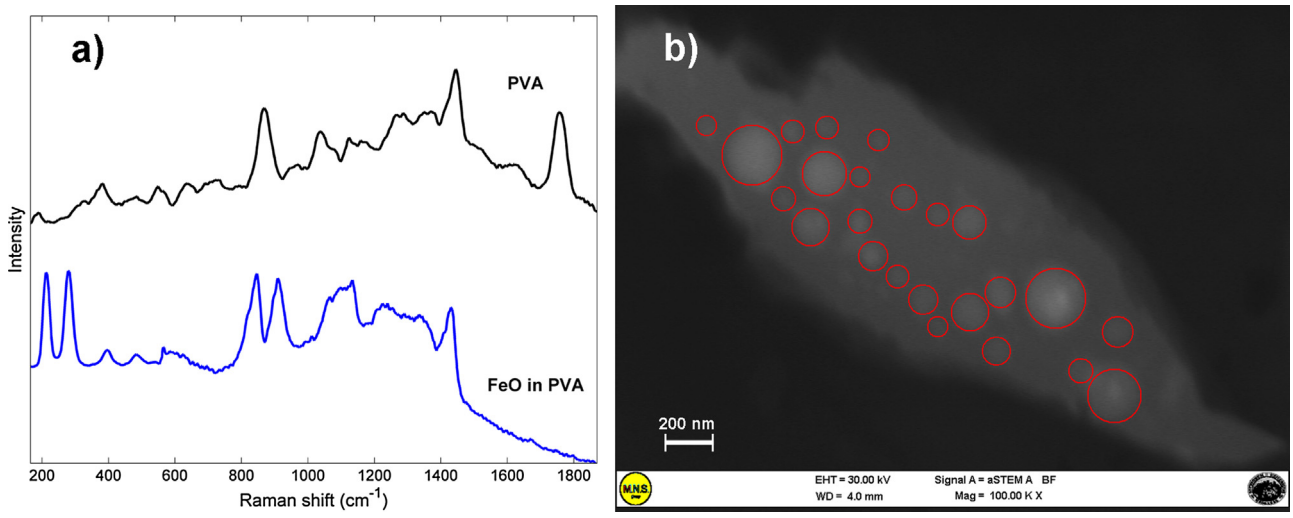

Fig. 3. (a) Raman spectrum of the iron oxide nanoparticles prepared in water in comparison to PVA Raman spectrum; (b) STEM images of the samples prepared in the PVA water solution.

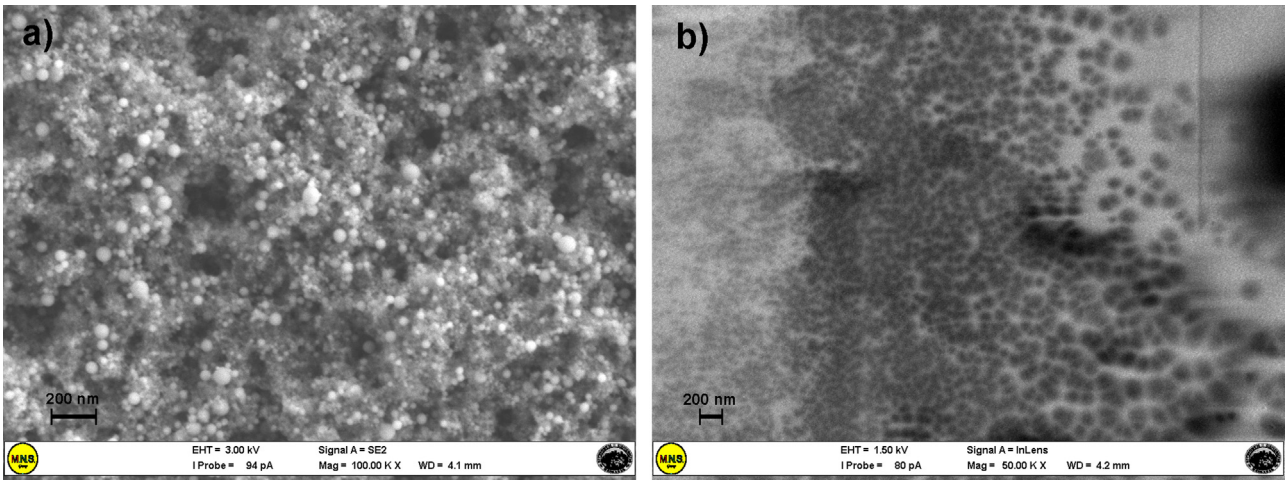

Fig. 4. SEM images of the samples prepared, at the laser power of 0.5 W, in water (a) and in PVA water solution (b).

(1.5 W). However, the nanocolloids prepared at this laser power start to precipitate after few hours from the ablation, while the solutions prepared at the lower laser power remain stable for some days. Hence, the optimal ablation time and laser power are 2 min and 0.5 W, respectively.

The structure of the iron oxide particles was defined carrying out Raman and X-ray photoelectron (XPS) measures. In Fig. 2a is shown the Raman spectrum of the sample prepared in water. It is characterized by some contributions centred at about 226.8, 292.5, 400, 486.5 and 600 cm^{-1}, ascribed to the Fe—O vibrational stretching modes in the hematite phase (α-Fe_2O_3). Really, the Raman features centred at 226.5 cm^{-1} is the convolution of the A_{1g} and $E_{g(1)}$ modes at 226 and 245 cm^{-1}. Analogously, the band centred at 292.5 cm^{-1} is due to the $E_{g(2)}$ and $E_{g(3)}$ vibrational modes, generally located at 293 and 298 cm^{-1}. Moreover, the Raman contributions, located at the higher wavenumber, refer to the $E_{g(4)}$, $A_{1g(2)}$ and $E_{g(5)}$ vibrational modes, expected at 410, 500 and 610 cm^{-1}, respectively [16]. The XPS analysis show the presence in the sample of C (39%), O (43%), Fe (16%), Na (1%) and Cl (1%). Information about the bonding fractions are obtained by the high resolution XPS profiles of the recorded atomic species. In Fig. 2b is shown the Fe 2p lineshape. This profile is characterized by two main contributions, ascribed to the Fe $2p_{3/2}$ and Fe $2p_{1/2}$ spin-orbit components, centred at 710.7 and 724.2 eV, respectively [17]. Moreover, it is evident the satellite peak at about 719 eV. According to these evidences, the hematite α-Fe_2O_3 and maghemite γ-Fe_2O_3 phases coexist in our sample. This is not in contradiction with the Raman data, whereas XPS is a technique that probes the surface layers, generally more oxidized.

Information about the particles dimensions and their distribution are obtained from the analysis of the SEM images and also by the DLS data. In Fig. 2a is shown a SEM image of the sample prepared in water at the laser power of 0.5 W while in Fig. 2b are reported the Fe_2O_3 particles dimensional distribution, estimated by the DLS data. SEM image shows spherical nanoparticles with dimensions ranging between 20 and 100 nm. These results are in good agreement with DLS evidences. Upon increasing the laser power from 0.1 W up to 1.3 W, a bimodal dimensional distribution is observed. The dimensions of the nanoparticles increase from 40 nm up to 1 μm, at the maximum laser power used. As well known from literature data [18], the dimension of the materials can be "controlled" by acting on the ablation parameters (ablation time, laser fluence etc. . .) but also with an appropriate choice of the solvent in which the ablation process occurred, known that the nanoparticles formation is strongly related to the nucleation time which, in turn, changes according to the medium in which the plasma expansion happens. Furthermore, it is known that, by increasing the plasma

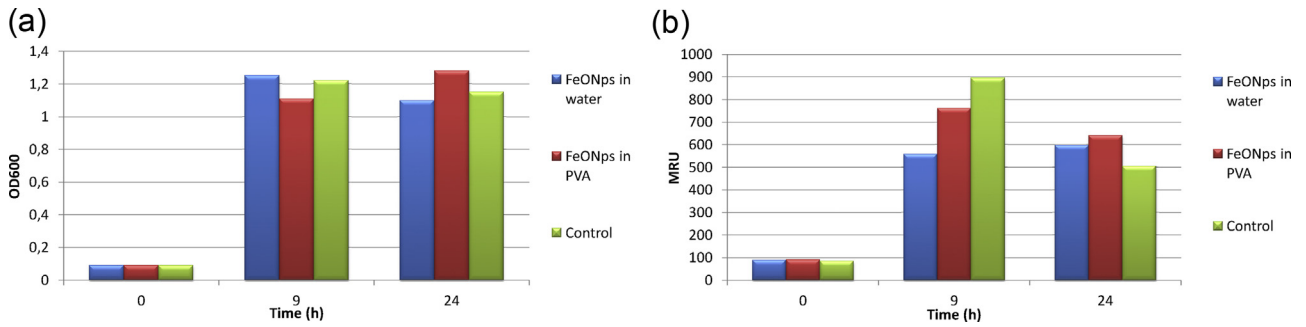

Fig. 5. (a) Optical density at 600 nm (OD_{600}) of *Staphylococcus aureus* in MHB medium supplemented with Fe_2O_3 in H_2O and in PVA; (b) MTT reduction unit (MRU) of *Staphylococcus aureus* in MHB medium supplemented with Fe_2O_3 in H_2O and in PVA.

confinement, decreases the nucleation time. Therefore, to investigate the possibility to further control the Fe_2O_3 nanoparticles distribution and dimensionality were carried out, under the same synthesis conditions used in water, some ablations of Fe target in an aqueous solution of polivininyl alcohol (PVA).

In Fig. 3 is shown the Raman spectrum of the sample prepared in PVA (for comparison the Raman spectrum of PVA is reported). The Raman spectrum of the sample shows the characteristic features of the hematite in the 200–300 cm^{-1} region, whose intensity is lower with respect to ones reported for the water ablated sample, and some of the PVA Raman contributions. On the overall, Raman results indicate that the hematite Fe_2O_3 phase characterize the samples, also in presence of a polymer environment. In this contest, to investigate about the confinement effect induced by the polymeric matrix which, in turn, determines the nanoparticles dimension and distribution, STEM characterizations were carried out. The Fe_2O_3 sample prepared in PVA shows spherical nanoparticles with size ranging between 5 and 10 nm (see Fig. 3b).

A further evidence of the effect of PVA on the nanoparticles size is given comparing SEM images of the samples prepared in water and in PVA water solution (see Fig. 4). An higher and uniform distribution of the Fe_2O_3 nanoparticles, whose size ranges between 5 and 10 nm, occurs in the polymer matrix with respect to what observed for the colloids prepared in water (sizes between 20 nm and 100 nm). As a general trend, we observe that, for the same ablation parameters (laser power and ablation time), the presence of PVA can significantly change the nanoparticles size and their distribution. Above all, it avoid nanoparticles aggregation process and its interface with a surrounding oxide shell. Finally, Zeta potential value, which measures the electrostatic potential that exists on the nanoparticles surface, reveals information regarding the surface charge and stability of the nanosystem. Both Fe_2O_3 nanoparticles prepared in water and in PVA show a negative charge. However, the Zeta potential values are very different: −30 mV (in water) and −8 mV (in PVA). The value estimated in PVA indicates a relative stability of the colloidal solution, ruling out the possibility of aggregation processes.

3.2. MTT reduction assay for anti-bacterial activity

Several studies report that iron nanoparticles exhibit antibacterial activity in dependence of their size, concentration and oxidation state [19], while the same does not occur in eukaryotic cells. The antibacterial activity of Fe_2O_3 nanoparticles prepared by pulsed laser ablation in water and in PVA aqueous solutions was assessed by a cell metabolic activity assay, using bacterial functional activities as an indicator of cell viability. According to the procedure described by Wang et al. [15], MTT reduction activity of *S. aureus* cultures, indicated by the parameter MRU (MTT reduction unit), can be estimated as follows:

$$\mathrm{MRU} = A_{550} \times \left(\frac{2500\mu\mathrm{L}}{200\mu\mathrm{L}}\right) \times \left(\frac{1000\mu\mathrm{L}}{200\mu\mathrm{L}}\right) \times \left(\frac{K}{\mathrm{OD}_{600}}\right) \quad (1)$$

where the terms A_{550}, OD_{600} and K indicate the optical absorption values of the cultures, at the wavelength of 550 nm, the optical density at the wavelength of 600 nm (per milliliter) and the dilution rate of the *S. aureus* samples, respectively. The formazan dissolution, related to the cellular metabolic activities, was tracked collecting the absorbance values at 500 nm (A_{550}) of formazan crystals formed within the 20 min of the reaction. Moreover, 200 μL is the volume of the *S. aureus* cell dilution, and 220 μL is the total volume of the mixture of 200 μL of cell and 20 μL of MTT stock. The presence of Fe_2O_3 nanoparticles (in absence of *S. aureus* culture) do not interfere with the MTT assay, as indicated by the optical absorption value acquired on the Fe_2O_3 nanoparticles incubated only with the medium (data not shown).

In Fig. 5a are shown the optical density values at 600 nm (OD_{600}) of *Staphylococcus aureus* in MHB medium, supplemented with Fe_2O_3 in H_2O and in PVA. No differences during the growth phase between Fe_2O_3 in water, Fe_2O_3 in PVA and in control sample is observed by the optical density value of the cultures. However, the respiratory activity of the cultures treated with iron nanoparticles in water and PVA is different, as observed by the absolute values of *S. aureus* MTT reduction unit (MRU) in MHB medium supplemented with Fe_2O_3 nanocolloids. MRU values as a function of time are shown in Fig. 5b. After 9 h of incubation, MRU values are significantly lower in the solution with Fe_2O_3 in water respect to the control sample. On the other hand, PVA–Fe_2O_3 solution has a minimum effect on *S. aureus* growth. Thus, the presence of PVA does not induce an additional toxic effect of bacteria growth in comparison to what reported in literature [20]. After 24 h, MRU values are not statistically different in all tested samples, indicating that the antibacterial activity of the water-Fe_2O_3 nanocolloids is partial. Furthermore, we outline that, for the water prepared sample, no significant MRU values differences occur between 9 h and 24 h while, in the control and PVA prepared samples, a decrement of the MRU values is evident at around 24 h (see Fig. 5b). This behaviour is explained taking into account the bacterial culture is in a stationary growth phase in which the respiratory activities are reduced. On the overall, iron oxide nanoparticles prepared by pulsed laser ablation in water show a partial bactericidal effect on Staphylococcus aureus. Conversely, a minimum effect is observed for the bacterial growth in the PVA–Fe_2O_3 nanocolloids. This behaviour could be due to the Fe_2O_3 nanoparticles surface properties given by the polymeric matrix around the single distributed iron oxide particles, in good agreement with Zeta potential data. However, the results reported in this work do not allow any more detailed explanation of these observations.Therefore, they can be regarded as prelimi-

nary results for a successive more systematic and comprehensive study of the PVA influence on the iron oxide surface properties. Nevertheless, being the PVA–Fe_2O_3 nanoparticles not toxic, they can be integrated in drug carrier multiblock-polymeric nanocomposites [21,22] and, in turn, they could be potentially employed to improve drug therapies.

4. Conclusion

Iron oxide nanoparticles were prepared in water and in a PVA water solutions. The synthesis, by means of a high-power picosecond laser ablation, allowed the preparation of iron oxide nanocolloids chemically and morphologically stable with a narrow size distribution, mainly in the polymeric matrix. Great efforts, to our best knowledge for the first time, have been done to correlate the samples properties which, in turn, are tailored by an appropriate choose of the ablation conditions in terms of laser power, ablation time and solvent, to the antibacterial activity. On the overall, it emerges that the laser ablation represents a fast and clean technique to obtain, in a one step and in a relatively short time (few minutes), hybrid polymer–Fe_2O_3 nanostructures with a well defined composition and morphology. Unlike the chemical approach, no post-preparation purification procedure is necessary adopting the pulsed laser ablation technique. Furthermore, the possibility to tailor the antibacterical activities of the iron oxide nanoparticles make them interesting materials for potential applications as efficient vectors for drug delivery and/or as constituent of specific platforms for drug targeting.

Acknowledgements

This work was partially funded by Italian Ministry of Education, University and Research (MIUR) by means of the national Program PON R&C 2007–2013, project “Hyppocrates–Sviluppo di Micro e Nano-Tecnologie e Sistemi Avanzati per la Salute dell’uomo (PON0200355)”. Authors also gratefully acknowledge financial support of A.B.A.L. onlus Messina (Italy) (http://abalmessina.it/) for the use of the XploRA Raman spectrometer.

References

[1] A.K. Gupta, M. Gupta, Synthesis and surface engineering of iron oxide nanoparticles for biomedical applications, Biomaterials 26 (18) (2005) 3995–4021.
[2] C.C. Berry, A.S.G. Curtis, Functionalisation of magnetic nanoparticles for applications in biomedicine, J. Phys. D Appl. Phys. 36 (2003) R198–R206.
[3] R.G.H. Beets-Tan, J.M.A. Van Engelshoven, J.W.M. Greve, Hepatic adenoma and focal nodular hyperplasia: MR findings with superparamagnetic iron oxide-enhanced MRI, Clin. Imaging 22 (3) (1998) 211–215.
[4] L. Babes, B. Denizot, G. Tanguy, J.J. Le Jeune, P. Jallet, Synthesis of iron oxide nanoparticles used as MRI contrast agents: a parametric study, J. Colloid Interface Sci. 212 (2) (1999) 474–482.
[5] D.C.F. Chan, D.B. Kirpotin, P.A. Bunn, Synthesis and evaluation of colloidal magnetic iron oxides for the site-specific radio frequency induced hyperthermia of cancer, J. Magn. Magn. Mater. 122 (1–3) (1993) 374–378.
[6] I. Brigger, C. Dubernet, P. Couvreur, Nanoparticles in cancer therapy and diagnosis, Adv. Drug Deliv. Rev. 54 (5) (2002) 631–651.
[7] F. Liu, S. Laurent, H. Fattahi, L.V. Elst, R.N. Muller, Superparamagnetic nanosystems based on iron oxide nanoparticles for biomedical imaging, Nanomedicine 6 (2011) 519–528.
[8] S.H. Joo, A.J. Feitz, D.L. Sedlak, T.D. Waite, Quantification of the oxidizing capacity of nanoparticulate zero-valent iron, Environ. Sci. Technol. 39 (2005) 1263–1268 [PubMed: 15787365].
[9] C.R. Keenan, D.L. Sedlak, Factors affecting the yield of oxidants from the reaction of nanoparticulate zero-valent iron and oxygen, Environ. Technol. 42 (4) (2008) 1262–1267.
[10] F. Dilnawaz, A. Singh, C. Mohanty, S.K. Sahoo, Dual drug loaded superparamagnetic iron oxide nanoparticles for targeted cancer therapy, Biomaterials 31 (2010) 3694–3706.
[11] M. Auffan, W. Achouak, J. Rose, M.A. Roncato, C. Chanéac, D.T. Waite, A. Masion, J.C. Woicik, M.R. Wiesner, J.Y. Bottero, Relation between the redox state of iron-based nanoparticles and their cytotoxicity toward *Escherichia coli*, Environ. Sci. Technol. 42 (2008) 6730–6735.
[12] M. Valodkar, P.S. Rathore, R.N. Jadeja, M. Thounaojam, R.V. Deokar, S. Thakore, Cytotoxicity evaluation and antimicrobial studies of starch capped water soluble copper nanoparticles, J. Hazard. Mater. 201–202 (2012) 244–249.
[13] Z.M. Xiu, Z.H. Jin, T.L. Li, S. Mahendra, G.V. Lowry, P.J.J. Alvarez, Effects of nano-scale zero-valent iron particles on a mixed culture dechlorinating trichloroethylene, Bioresour. Technol. 101 (2010) 1141–1146.
[14] S.A. Mahdy, Q.J. Raheed, P.T. Kalaichelvan, Antimicrobial activity of zero-valent iron nanoparticles, Int. J. Mod. Eng. Res. 2 (2012) 578–581.
[15] H. Wang, H. Cheng, F. Wang, D. Wei, X. Wang, An improved 3-(4,5-dimethylthiazol-2-yl)-2,5-diphenyl tetrazolium bromide (MTT) reduction assay for evaluating the viability of *E. coli* cells, J. Microbiol. Methods 82 (2010) 330–333.
[16] S.H. Shime, T.S. Duffy, Raman spettroscopy of Fe_2O_3 to 62GPa, Am. Miner. 87 (2001) 318–326.
[17] V. Rebuttini, E. Fazio, S. Santangelo, F. Neri, G. Caputo, C. Martin, T. Brousse, F. Favier, N. Pinna, Chemical modification of graphene oxide through diazonium chemistry and its influence on the structure-properties relationships of graphene oxide–iron oxide nanocomposites, Chem.—Eur. J. 21 (2015) 1–11.
[18] E. Fazio, F. Barreca, S. Spadaro, G. Currò, F. Neri, Preparation of luminescent and optical limiting silicon nanostructures by nanosecond-pulsed laser ablation in liquids, Mater. Chem. Phys. 130 (2011) 418–424.
[19] E. Barzan, S. Mehrabian, S. Irian, Antimicrobial and genotoxicity effects of zero-valent iron nanoparticles, Jundishapur J. Microbiol. 7 (5) (2014) e10054.
[20] J.A.S. Salman, M.F.H. Kadhemy, M. SamiJaleel, A.K. Abdal, Effect of PVA, PVA/biosurfactant on some pathogenic bacteria in glass and plastic plates, Int. J. Curr. Microbiol. Appl. Sci. 3 (10) (2014) 301–309.
[21] E. Fazio, A. Scala, S. Grimato, A. Ridolfo, G. Grassi, F. Neri, Laser light triggered smart release of silibinin from a PEGylated–PLGA gold nanocomposite, J. Mater. Chem. B 3 (2015) 9023–9032.
[22] J. Estelrich, E. Escribano, J. Queralt, M.A. Busquets, Iron oxide nanoparticles for magnetically-guided and magnetically-responsive drug delivery, Int. J. Mol. Sci. 16 (2015) 8070–8101.